Received February 26, 2022, accepted March 17, 2022, date of publication March 24, 2022, date of current version March 30, 2022.

Digital Object Identifier 10.1109/ACCESS.2022.3161974

The Probability Density Function of Bearing Obtained From a Cartesian-to-Polar Transformation

KEVIN R. FORD[1], (Member, IEEE), AND ANTON J. HAUG[2], (Life Member, IEEE)
[1]Applied Physics Laboratory, Johns Hopkins University, Laurel, MD 20723, USA
[2]Applied Physics Laboratory, Johns Hopkins University, Laurel, MD 20723, USA *(Retired)*

Corresponding author: Kevin R. Ford (kevin.ford@jhuapl.edu)

ABSTRACT The problem of tracking a two-dimensional Cartesian state of a target using polar observations is well known. At a close range, a traditional extended Kalman filter (EKF) can fail owing to nonlinearity introduced by the Cartesian-to-polar transformation in the observation prediction step of the filter. This is a byproduct of the nonlinear transformation acting on the state variables, which make up a bivariate Gaussian distribution. The nonlinear transformation in question is the arctangent of Cartesian state variables X and Y, which corresponds to the target bearing. At long range, the bearing behaves as a wrapped Gaussian random variable, and behaves well for the EKF. At close range, the bearing is shown to be non-Gaussian, converging to the wrapped uniform distribution when X and Y are uncorrelated. This study provides a concise derivation of the probability density function (PDF) for bearing for the EKF observation prediction step and explores the limiting behavior for this distribution while parameterizing the target range.

INDEX TERMS Bearing, Gaussian, Kalman filter, PDF.

I. INTRODUCTION

In radar target tracking applications [2], [3], [9], a Kalman filter (KF) is often used to track objects within the field of view of a sensor. In this context, sensors typically deliver measurements in polar coordinates. However, the state vector of the object being tracked is typically defined in Cartesian coordinates. This necessitates a Cartesian to polar transformation to make predictions for the sensor measurements.

The azimuthal angle, or bearing, can be computed using only the coordinates in the east-north (EN) plane; the coordinate system is shown in Fig. 1. This coordinate transformation requires one to take an inverse tangent

$$\Theta = \arctan\left(\frac{X}{Y}\right), \tag{1}$$

where X and Y are elements of a vector $\boldsymbol{X}$ and compose the bivariate Gaussian distribution

$$\boldsymbol{X} \sim \mathrm{N}(\boldsymbol{\mu}, \boldsymbol{\Sigma}), \tag{2}$$

where the mean and covariance are

$$\boldsymbol{\mu} = \begin{bmatrix} \mu_X & \mu_Y \end{bmatrix}^{\mathrm{T}}, \tag{3}$$

and

$$\boldsymbol{\Sigma} = \begin{bmatrix} \sigma_X^2 & \rho\sigma_X\sigma_Y \\ \rho\sigma_X\sigma_Y & \sigma_Y^2 \end{bmatrix}. \tag{4}$$

The bearing of the target (Θ) described in (1) is a random variable that behaves as a wrapped Gaussian [19] at long range. For Sections II and III random variables are referred to with capital letters, whereas deterministic variables are lower-case.

When the target approaches the origin (collocated with the sensor), the variance increases, and the distribution for Θ resembles a uniform $(-\pi, \pi]$ random variable. As the behavior becomes less Gaussian, the bearing prediction begins to diverge and can lead to poor tracking accuracy for the KF. This problem can be ameliorated using a debiased converted measurement filter [1], [3], [16], which converts the polar measurements to Cartesian coordinates prior to executing the algorithm. Another approach is to maintain the filter state in polar coordinates, as was done in [10] and [11], thereby avoiding polar-to-Cartesian conversion in exchange for maintaining a nonlinear dynamic model. A third alternative is to use observation only (O2) inference to infer the state directly from the observations [17].

The associate editor coordinating the review of this manuscript and approving it for publication was Derek Abbott.

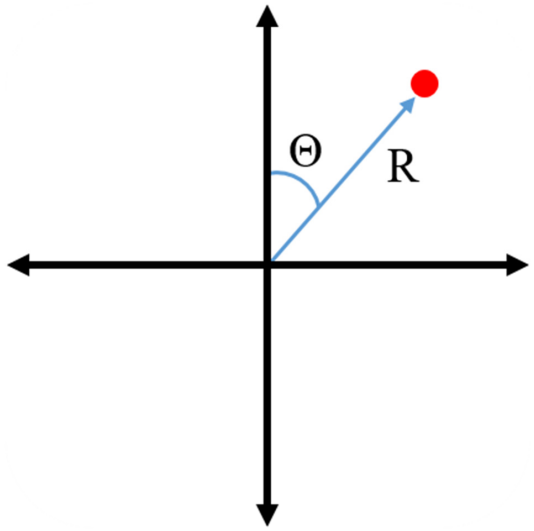

FIGURE 1. The two dimensional coordinate system used for this paper, where R denotes range and θ denotes azimuth (bearing) angle from North.

The Monte Carlo samples of X and Y for a radially inbound trajectory drawn from the PDF given in (2) are shown in the left half of Fig. 2. For simplicity, X and Y are considered uncorrelated with equal variance for this example. Clearly, the bearing samples calculated from the Cartesian samples using (1) diverge at close range, as shown in the right half of Fig. 2.

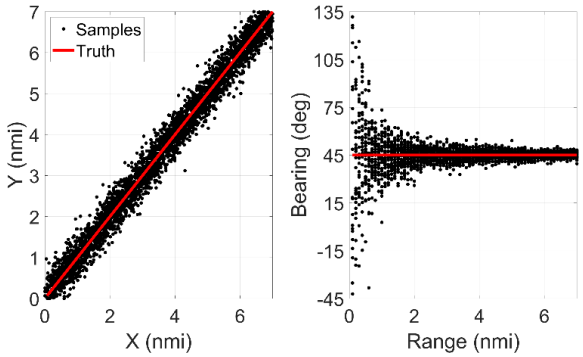

FIGURE 2. Plot of radially inbound target (45 degrees from North, $\sigma = 0.2$ data miles); Cartesian Gaussian samples (left) and computed bearing samples (right).

The available literature has already explored aspects of the distributions resulting from the Cartesian to polar transformation [12]. For instance, the Cauchy distribution is also the ratio distribution for two independent, zero-mean Gaussian-distributed random variables. Several authors have performed statistical analyses of the Cauchy distribution [4], [20], but the arctangent of a Cauchy distributed random variable only represents the end-game behavior of Θ at the zero range and assumes that X and Y are independent.

Other authors have explored the properties of the arctangent distribution and its relationship with the folded standard Gaussian distribution [22]. These results have value, but do not address the more general wrapped Gaussian distribution or its application to target tracking performance.

While we focus on the target bearing in this study, it should be noted that for the target range (R) given by

$$R = \sqrt{X^2 + Y^2}, \tag{5}$$

where X and Y are drawn from (2), and the probability distribution is a bivariate non-central chi distribution [15]. This distribution simplifies to the well-known Rice distribution [23] when X and Y are independent, with equal variance σ^2.

$$R \sim \text{Rice}\,(\mu_{\text{R}}, \sigma), \tag{6}$$

where

$$\mu_{\text{R}} = \sqrt{\mu_{\text{X}}^2 + \mu_{\text{Y}}^2}. \tag{7}$$

In the following sections, we focus on the derivation of the PDF of the bearing and its effect on the Kalman filter performance. The derivation is presented in Section II. The asymptotic behavior of the distribution as the target approaches the origin is examined in Section III. The implications of the asymptotic behavior of the bearing for a Cartesian EKF with polar measurements are discussed in IV.

II. DERIVATION OF THE PROBABILITY DENSITY FUNCTION FOR BEARING

Some authors, such as Haug, have already attempted to derive a density similar to the one desired here. However, the precise PDF for the bearings was not properly determined in [8] and [9]. Improper use of the direct transformation given in (1) causes a loss of sign information when taking the quotient of two variables because the inverse tangent function is periodic over $(-\pi/2,\pi/2)$, not the full circle. Mallick [18] pointed out in a recent note that the true transformation used in many tracking applications is the four-quadrant inverse tangent, despite many books, journals, and conferences writing the measurement function as in (1). In practice, a four-quadrant inverse tangent (such as that used in MATLAB) is used.

Using the two-quadrant inverse tangent, as Haug did in [8], [9] results in PDFs with peaks centered on the true bearing as well as the true bearing $\pm\pi$, as shown in Fig. 3. Further analysis shows that the PDF in [9] integrates to two over the full support, disqualifying it as a true PDF.

This study uses simple polar relations and variable transformations to obtain the PDF of a bearing random variable derived from a Cartesian to polar transformation. The PDF for the bearing can be used to assess the viability of the Gaussian assumption for the bearing as a function of range.

The development of the PDF for bearing begins with the polar-to-Cartesian transformations of R and Θ into X and Y in an EN coordinate system given by

$$X = R\sin(\Theta), \tag{8}$$

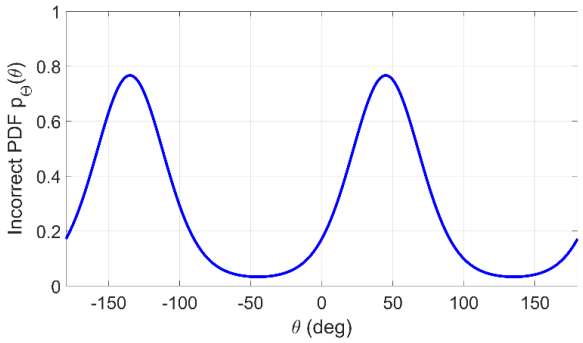

FIGURE 3. Incorrect application of inverse tangent function to obtain PDF for Φ results in double peaks ($\mu_X = \mu_Y = 3$ and $\sigma = 2$ for this example).

and

$$Y = R\cos(\Theta). \tag{9}$$

For convenience later in the derivation, it was helpful to redefine the mean values of X and Y in terms of their polar equivalents. Specifically, we define a mean target range μ_R with (7) and mean bearing μ_Θ such that

$$\mu_X = \mu_R \sin(\mu_\Theta), \tag{10}$$

and

$$\mu_Y = \mu_R \cos(\mu_\Theta), \tag{11}$$

with

$$\mu_\Theta = \arctan\left(\frac{\mu_X}{\mu_Y}\right). \tag{12}$$

The joint distribution for X and Y can be written as

$$f_{XY}(x,y) = \frac{1}{2\pi\sigma_X\sigma_Y\sqrt{1-\rho^2}} \exp\left[-\frac{z(x,y)}{2\left(1-\rho^2\right)}\right], \tag{13}$$

where

$$z(x,y) \equiv \frac{(x-\mu_X)^2}{2\sigma_X^2} + \frac{(y-\mu_Y)^2}{2\sigma_Y^2} - \frac{2\rho(x-\mu_X)(y-\mu_Y)}{\sigma_X\sigma_Y}. \tag{14}$$

Substituting the results of (8)-(12) into (13) yields

$$f_{XY}(x(r,\theta), y(r,\theta)) = \frac{1}{2\pi\sigma_X\sigma_Y\sqrt{1-\rho^2}} \times \exp\left[-\frac{a(\theta)r^2 - b(\theta)r + c}{d}\right] \tag{15}$$

where

$$a(\theta) = \frac{\sin^2(\theta)}{\sigma_X^2} + \frac{\cos^2(\theta)}{\sigma_Y^2} - \frac{\rho\sin(2\theta)}{\sigma_X\sigma_Y}; \tag{16}$$

$$b(\theta) = 2\mu_R\left(\frac{\sin(\mu_\Theta)\sin(\theta)}{\sigma_X^2} + \frac{\cos(\mu_\Theta)\cos(\theta)}{\sigma_Y^2}\right) - \frac{2\rho\mu_R\sin(\theta+\mu_\Theta)}{\sigma_X\sigma_Y}; \tag{17}$$

$$c = \mu_R^2\left(\frac{\sin^2(\mu_\Theta)}{\sigma_X^2} + \frac{\cos^2(\mu_\Theta)}{\sigma_Y^2} - \frac{\rho\sin(2\mu_\Theta)}{\sigma_X\sigma_Y}\right); \tag{18}$$

$$d = 2\left(1-\rho^2\right). \tag{19}$$

A change of variable [5] can now be performed to obtain the joint distribution in polar coordinates, $f_{R\Theta}(r,\theta)$, using

$$f_{R\Theta}(r,\theta) = |J(r,\theta)|\, f_{XY}(x(r,\theta), y(r,\theta)) \tag{20}$$

where $J(r,\theta)$ is the Jacobian [21] of the transformation equations (8)–(9) given by:

$$J(r,\theta) = \begin{vmatrix} \frac{\partial(r\sin(\theta))}{\partial r} & \frac{\partial(r\sin(\theta))}{\partial\theta} \\ \frac{\partial(r\cos(\theta))}{\partial r} & \frac{\partial(r\cos(\theta))}{\partial\theta} \end{vmatrix} = -r. \tag{21}$$

This leads to

$$f_{R\Theta}(r,\theta) = \frac{r}{2\pi\sigma_X\sigma_Y\sqrt{1-\rho^2}} \times \exp\left[-\frac{1}{d}\left(a(\theta)r^2 - b(\theta)r + c\right)\right]. \tag{22}$$

The joint PDF for R and Θ can be simplified by completing the square in the exponential argument to obtain

$$f_{R\Theta}(r,\theta) = \frac{r}{2\pi\sigma_X\sigma_Y\sqrt{1-\rho^2}} \exp\left[c - \frac{b^2(\theta)}{4a(\theta)}\right] \times \exp\left[-\frac{a(\theta)}{d}\left(r - \frac{b(\theta)}{a(\theta)}\right)^2\right]. \tag{23}$$

To obtain the marginal PDF of Θ, we integrate (22) with the support of R, resulting in:

$$f_\Theta(\theta) = \int_0^\infty f_{R\Theta}(r,\theta)dr = \frac{1}{2\pi\sigma_X\sigma_Y\sqrt{1-\rho^2}} \exp\left[\frac{c}{d} - \frac{b^2(\theta)}{4a(\theta)d}\right] \times \int_0^\infty r\exp\left[-\frac{a(\theta)}{d}\left(r - \frac{b(\theta)}{a(\theta)}\right)^2\right]dr. \tag{24}$$

Using standard integral methods or referring to [6], we can obtain the marginal distribution for Θ:

$$f_\Theta(\theta) = \frac{1}{2\pi a(\theta)\sigma_X\sigma_Y\sqrt{1-\rho^2}} \times \exp\left(\frac{c}{d} - \frac{b^2(\theta)}{4a(\theta)d}\right)\left[\frac{d}{2}\exp\left(\frac{b^2(\theta)}{a(\theta)d}\right) + b(\theta)\sqrt{\frac{\pi d}{a(\theta)}}\Phi\left(b(\theta)\sqrt{\frac{2}{a(\theta)\,d}}\right)\right], \tag{25}$$

where (x) is the cumulative distribution function (CDF) of the standard Gaussian distribution N(0,1).

When X and Y are uncorrelated ($\rho = 0$) with equal variance ($\sigma_X = \sigma_Y = \sigma$), equation (27) simplifies to

$$f_\Theta(\theta) = \frac{1}{2\pi}\exp\left[-\frac{\mu_R^2}{2\sigma^2}\right] + \frac{\alpha(\theta)}{\sqrt{2\pi\sigma^2}}\exp\left[-\frac{\mu_R^2 - \alpha(\theta)^2}{2\sigma^2}\right]\Phi\left(\frac{\alpha(\theta)}{\sigma}\right). \tag{26}$$

where

$$\alpha(\theta) \equiv \mu_R \cos(\theta - \mu_\Theta). \tag{27}$$

The asymptotic behaviors of the general PDF (25) and simplified PDF (26) are discussed in Section III.

III. ASYMPTOTIC BEHAVIOR OF THE BEARING DISTRIBUTION

The mixed uniform and Gaussian behavior of the distribution given in Equation (26) may not be immediately obvious. It only becomes so by observing the asymptotic behavior of each term in (26) with respect to μ_R. The first term of (26) is designated as $f_\Theta{}^{(1)}(\theta)$, and the second term as $f_\Theta{}^{(2)}(\theta)$. Let

$$f_\Theta^{(1)}(\theta) = \frac{1}{2\pi}\exp\left[-\frac{\mu_R^2}{2\sigma^2}\right]. \tag{28}$$

Now it is more easily shown that

$$\lim_{\mu_R\to 0}\frac{1}{2\pi}\exp\left[-\frac{\mu_R^2}{2\sigma^2}\right] = \frac{1}{2\pi} \tag{29}$$

and

$$\lim_{\mu_R\to\infty}\frac{1}{2\pi}\exp\left[-\frac{\mu_R^2}{2\sigma^2}\right] = 0. \tag{30}$$

Thus, as μ_R approaches zero, $f_\Theta{}^{(1)}(\theta)$ becomes a wrapped uniform PDF over $(-\pi, \pi]$, whereas as μ_R approaches infinity, $f_\Theta{}^{(1)}(\theta)$ vanishes.

Now examine the second term in (26) and define

$$f_\Theta^{(2)}(\theta) = \frac{\alpha(\theta)}{\sqrt{2\pi\sigma^2}}\exp\left[-\frac{\mu_R^2 - \alpha(\theta)^2}{2\sigma^2}\right]\Phi\left(\frac{\alpha(\theta)}{\sigma}\right). \tag{31}$$

From (27) it is clear that $\alpha(\theta)$ approaches zero as μ_R approaches zero because $\alpha(\theta)$ is linear with respect to μ_R. Therefore, as μ_R approaches zero,

$$\lim_{\mu_R\to 0}\frac{\alpha(\theta)}{\sqrt{2\pi\sigma}}\exp\left[-\frac{\mu_R^2 - \alpha(\theta)^2}{2\sigma^2}\right]\Phi\left(\frac{\alpha(\theta)}{\sigma}\right) = 0. \tag{32}$$

Thus

$$\lim_{\mu_R\to 0} f_\Theta^{(2)}(\theta) = 0, \tag{33}$$

and the result for the distribution when X and Y are uncorrelated with equal variance is:

$$\lim_{\mu_R\to 0} f_\Theta(\theta) \to \mathrm{U}(-\pi, \pi). \tag{34}$$

The standard normal CDF also exhibits simple behavior in limiting cases, such that it approaches constant scaling factors.

$$\lim_{\mu_R\to 0}\Phi\left(\frac{\alpha(\theta)}{\sigma}\right) = \frac{1}{2} \tag{35}$$

and

$$\lim_{\mu_R\to\infty}\Phi\left(\frac{\alpha(\theta)}{\sigma}\right) = 1. \tag{36}$$

As μ_R increases, the influence of $f_\Theta{}^{(2)}(\theta)$ becomes more pronounced. Taking the Taylor series expansion of the leading term in (31) about μ_Θ yields:

$$\frac{\alpha(\theta)}{\sigma\sqrt{2\pi}} = \frac{\mu_R}{\sigma\sqrt{2\pi}}\left[1 - \frac{1}{2}(\theta - \mu_\Theta)^2 + \ldots\right]. \tag{37}$$

For θ near μ_Θ (37) reduces to

$$\frac{\alpha(\theta)}{\sqrt{2\pi}\sigma} \approx \frac{\mu_R}{\sqrt{2\pi}\sigma}. \tag{38}$$

Similarly, the exponential term in (31) becomes

$$\frac{\mu_R^2 - \alpha(\theta)^2}{2\sigma^2} \approx \frac{\mu_R^2}{2\sigma^2}(\theta - \mu_\Theta)^2. \tag{39}$$

By applying the approximations in (38) and (39) to (31) we can find the limit of $f_\Theta{}^{(2)}(\theta)$ as μ_R approaches infinity:

$$\lim_{\mu_R\to\infty} f_\Theta^{(2)}(\theta) \approx \frac{1}{\sqrt{2\pi}\left(\frac{\sigma}{\mu_R}\right)}\exp\left[-\frac{(\theta - \mu_\Theta)^2}{2\left(\frac{\sigma}{\mu_R}\right)^2}\right]. \tag{40}$$

Because $f_\Theta{}^{(1)}(\theta)$ vanishes for large μ_R and $f_\Theta{}^{(2)}(\theta)$ can be approximated using (40), the PDF of the bearing at long ranges can be written as a (wrapped) Gaussian distribution:

$$\lim_{\mu_R\to\infty} f_\Theta(\theta) \to \mathrm{N}\left(\mu_\Theta, \left(\frac{\sigma}{\mu_R}\right)^2\right). \tag{41}$$

A simple test can be used to demonstrate that the PDF of Θ behaves like the wrapped Gaussian distribution in (41). Fig. 4 shows that as the ratio μ_R/σ increases (where the true σ is constant), the sample standard deviation (represented by the blue dots in Fig. 4) quickly converges to the approximated standard distribution. From the plot in Fig. 4, the difference becomes indistinguishable at approximately $\mu_R/\sigma = 5$. The approximated standard deviation was obtained by taking the square root of the variance from (43), whereas the true standard deviation refers to the standard deviation of the samples found on the right-hand side of Fig. 2.

A plot of the bearing PDF from Equation (26) for various bearing values and mean ranges is shown in Fig. 5. A careful inspection of the plot in Fig. 5 reveals that the distribution is a wrapped Gaussian centered on the nominal bearing ($\mu_\Theta = 45°$) when μ_R is large. It can be seen that as μ_R decreases the PDF transitions from that of a wrapped Gaussian with support $(-\pi, \pi]$ to Uniform over the same support.

The asymptotic behavior of the generalized version of the distribution (25) is not as convenient as that of the

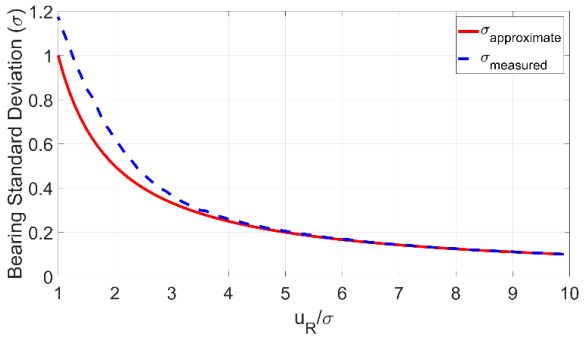

FIGURE 4. Plot depicting sample standard deviation and its approximation found by taking the square root of the variance for the wrapped Gaussian distribution.

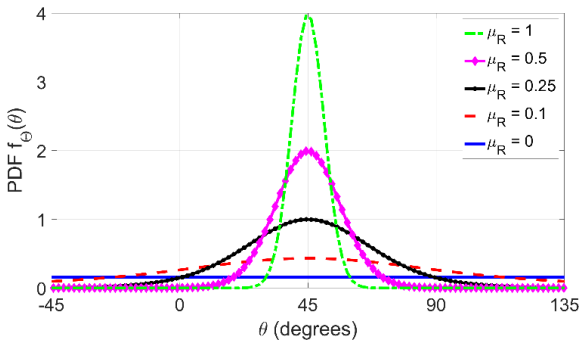

FIGURE 5. Plot of the bearing PDF for various values of μ_R with constant $\sigma = 0.1$ as the standard deviation.

simplified version. At long range, the distribution is somewhat similar to a wrapped Gaussian, but for the sake of simplicity, this paper will focus on the behavior of the distribution at close range. The key finding from this section relates to the expected value of the distribution

$$\lim_{\mu_R \to 0} \mathrm{E}[\Theta] = 0. \tag{42}$$

The conclusion drawn in (42) is clear for the simple case presented in (34) when the distribution approaches uniform over $(-\pi, \pi]$. Determining the expected value for a general distribution requires additional computation.

The limiting behavior for each of the scalar values presented in (16)–(19) is simple to determine,

$$\lim_{\mu_R \to 0} \mathrm{a}(\theta) = \frac{\sin^2(\theta)}{\sigma_X^2} + \frac{\cos^2(\theta)}{\sigma_Y^2} - \frac{\rho \sin(2\theta)}{\sigma_X \sigma_Y} \tag{43}$$

$$\lim_{\mu_R \to 0} \mathrm{b}(\theta) = 0, \tag{44}$$

$$\lim_{\mu_R \to 0} c = 0, \tag{45}$$

$$\lim_{\mu_R \to 0} d = 2\left(1 - \rho^2\right). \tag{46}$$

At close range the general distribution becomes

$$\lim_{\mu_R \to 0} \mathrm{f}_\Theta(\theta) = \frac{d}{4\pi \mathrm{a}(\theta) \sigma_X \sigma_Y \sqrt{1-\rho^2}}. \tag{47}$$

The right-hand side of (47) is a function of θ because of the presence of $\mathrm{a}(\theta)$, and is unlike (34). However, simple trigonometric identities can be used to show that $\mathrm{a}(\theta)$ is

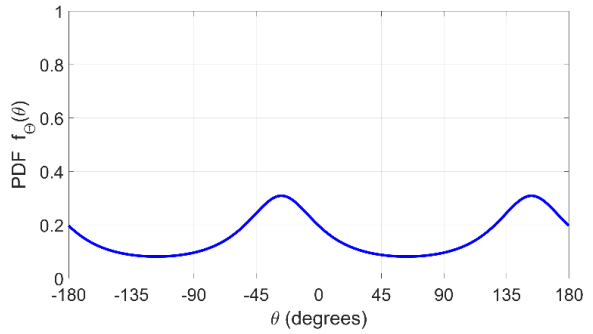

FIGURE 6. Plot of the bearing PDF at $\mu_R = 0$ with $\sigma_X = 0.7$, $\sigma_Y = 1.0$, and $\rho = -0.5$.

twice periodic over $(-\pi, \pi]$. Thus, (42) also applies to the generalized version of the distribution in (25).

This result can also be computed explicitly using the method to find the moments of wrapped random variables [19]. An example of the distribution at zero range is shown in Fig. 6.

Curiously, the distribution for the case in Fig. 6 resembles the incorrect distribution shown in Fig. 3. However, the dual peaks in Fig. 3 are due to the ambiguity introduced by the arctangent function in general, while the peaks in Fig. 6 are artifacts caused by $\mathrm{a}(\theta)$. This distribution also integrates to unit area, unlike the incorrect distribution presented earlier.

In the next section, it will be shown how (42) impacts the Kalman filter position estimates and causes them to become lose accuracy at close ranges.

IV. IMPACT ON KALMAN FILTER PERFORMANCE

The Kalman filter algorithm is well known to perform optimally for linear functions of Gaussian distributed variables [13]. A Cartesian KF, which relies on measurements in polar coordinates, clearly violates the linearity requirement owing to nonlinear functions (1) and (5).

The state model is described by

$$\boldsymbol{x}_n = \mathbf{f}(\boldsymbol{x}_{n-1}) + \boldsymbol{v}_{n-1}, \tag{48}$$

where the vector $\boldsymbol{v}$ is zero-mean Gaussian distributed with covariance $\boldsymbol{Q}$. The state vector (including the velocity terms) is assumed to be

$$\boldsymbol{x}_n = \begin{bmatrix} x_n & y_n & \dot{x}_n & \dot{y}_n \end{bmatrix}^T \tag{49}$$

where x_n and y_n represent the Cartesian position of the target at time n. Note that in this section, bold lower case letters refer to vectors, while bold upper case letters refer to matrices.

Using the constant velocity (CV) assumption for the state model, the function $\mathbf{f}(\boldsymbol{x})$ is linear as follows:

$$\mathbf{f}(\boldsymbol{x}_{n-1}) = \boldsymbol{F}\boldsymbol{x}_{n-1}. \tag{50}$$

The state transition matrix $\mathbf{F}$ for this model is

$$\boldsymbol{F} = \begin{bmatrix} 1 & 0 & \Delta t & 0 \\ 0 & 1 & 0 & \Delta t \\ 0 & 0 & 1 & 0 \\ 0 & 0 & 0 & 1 \end{bmatrix}, \tag{51}$$

where Δt is the time difference between measurement updates.

The state ($\hat{\boldsymbol{x}}$) and error covariance ($\boldsymbol{P}^{xx}$) predictions at time n based on observations up to time n-1 are also linear for the CV model:

$$\hat{\boldsymbol{x}}_{\mathrm{n|n-1}} = \boldsymbol{F}\hat{\boldsymbol{x}}_{\mathrm{n-1|n-1}}, \tag{52}$$

$$\boldsymbol{P}^{\mathrm{xx}}_{\mathrm{n|n-1}} = \boldsymbol{F}\boldsymbol{P}^{\mathrm{xx}}_{\mathrm{n-1|n-1}}\boldsymbol{F}^{\mathrm{T}} + \boldsymbol{Q}_{\mathrm{n}}, \tag{53}$$

where $\boldsymbol{Q}_{\mathrm{n}}$ is the process noise matrix. Assuming that the target is equally maneuverable in all directions and the measurement update period is constant, the process noise matrix becomes

$$\boldsymbol{Q} = \begin{bmatrix} \frac{q(\Delta t)^3}{3} & 0 & \frac{q(\Delta t)^2}{2} & 0 \\ 0 & \frac{q(\Delta t)^3}{3} & 0 & \frac{q(\Delta t)^2}{2} \\ \frac{q(\Delta t)^2}{2} & 0 & q(\Delta t) & 0 \\ 0 & 0 & 0 & q(\Delta t) \end{bmatrix}, \tag{54}$$

where q denotes the process noise intensity. In practice, the process noise intensity is selected by the filter developer to account for the uncertainty of the dynamic model. This tuning parameter directly influences the position variance terms on the main diagonal of the predicted covariance (53).

The observation model is

$$z_{\mathrm{n}} = \mathbf{h}(\boldsymbol{x}_{\mathrm{n}}) + \boldsymbol{w}_{\mathrm{n}}, \tag{55}$$

where the vector $\boldsymbol{w}$ is Gaussian distributed with zero mean and covariance matrix $\boldsymbol{S}$ and is assumed to be independent of $\boldsymbol{v}$. The covariance matrix for the observations is often treated as independent for the range and bearing measurements

$$\boldsymbol{S} = \begin{bmatrix} \sigma_{\mathrm{R}}^2 & 0 \\ 0 & \sigma_{\Theta}^2 \end{bmatrix}. \tag{56}$$

The observation model is the same pair of nonlinear functions discussed previously

$$\mathbf{h}(\boldsymbol{x}_{\mathrm{n}}) = \begin{bmatrix} r_{\mathrm{n}} \\ \theta_{\mathrm{n}} \end{bmatrix} = \begin{bmatrix} \sqrt{x_{\mathrm{n}}^2 + y_{\mathrm{n}}^2} \\ \arctan\left(x_{\mathrm{n}}/y_{\mathrm{n}}\right) \end{bmatrix} \tag{57}$$

In Section III it was shown that the resulting distribution for the bearing will appear Gaussian at long range, and progressively less Gaussian as μ_{R} shrinks. Given the knowledge of the probability density of the target state for all prior measurements $\mathrm{p}(\boldsymbol{x}_{\mathrm{n}}|\boldsymbol{z}_{1:\mathrm{n}-1})$, the predicted bearing approaches zero at close range,

$$\hat{\boldsymbol{z}}_{\mathrm{n|n-1}} = \begin{bmatrix} \int_{\Omega_{\mathbf{x}}} \sqrt{x_{\mathrm{n}}^2 + y_{\mathrm{n}}^2}\,\mathrm{p}(\boldsymbol{x}_{\mathrm{n}}|\boldsymbol{z}_{1:\mathrm{n}-1})\mathrm{d}\boldsymbol{x}_{\mathrm{n}} \\ 0 \end{bmatrix}. \tag{58}$$

The residual vector ξ_{n} for the filter is

$$\boldsymbol{\xi}_n = \mathbf{z}_n^{\mathrm{o}} - \hat{\mathbf{z}}_{n|n-1}, \tag{59}$$

using the latest observation data, $z_{\mathrm{n}}^{\mathrm{o}}$. The residual in the bearing dimension increases as the bearing predictions become uniformly randomly distributed. Residual growth of this nature is indicative of a poorly matched model to the tracking problem, and may result in poor tracking performance [7].

Another key takeaway is that increasing the process noise has the same effect as decreasing μ_{R}, and vice versa, because of its direct impact on the variance terms in (16)–(18). This means that a filter designer can unintentionally decrease the accuracy of their EKF if they are not judicious in their selection of the tuning parameter q given their measurement update period constraints.

In many target-tracking applications, target maneuvers are not known a priori; therefore, they are often modeled as random accelerations in the CV model. A filter designer focused on tracking a maneuvering inbound target must include appropriate levels of process noise to account for these maneuvers based on the knowledge of the target's maneuverability. However, a combination of large process noise and closing the target range can have a negative impact on the filter performance owing to the combination of nonlinear and non-Gaussian behavior of the bearing model.

Many have chosen to address the nonlinearity of $\mathbf{h}(\boldsymbol{x}_{\mathrm{n}})$ for mixed Cartesian and polar tracking problems using the EKF [11], [14], [24]. In the EKF formulation, the estimate of (55) is simplified as

$$\hat{\boldsymbol{z}}_{\mathrm{n|n-1}} = \mathbf{h}\left(\hat{\boldsymbol{x}}_{\mathrm{n|n-1}}\right). \tag{60}$$

However, linearizing the filter about the state and covariance does not address the fact that, at a close range, the arctangent function is still quite nonlinear.

To demonstrate the effects of range and process noise on the tracking performance, a series of simple experiments were performed using a CV Cartesian EKF to track a simulated radially inbound target (approaching the sensor origin at a 45° angle clockwise from north) with range and bearing measurements. In a real target tracking application, such as tracking a CV inbound anti-ship missile with a naval radar, expected target maneuvers must be modeled to stay within the process noise. No a priori knowledge of the maneuver is available to the tracker, so the process noise must encompass the largest possible deviations from the CV model. However, if the target executes no maneuver, it is easy to accidentally set the process noise intensity too high.

For this experiment, RMS position error statistics were collected over the course of 100 Monte Carlo runs, where measurements were generated by adding Gaussian random errors consistent with Equation (56) to the truth trajectory. For simplicity, and to highlight the plight of the target tracking filter designer, no process noise was added to the target trajectory. Fig. 7 demonstrates the impact of the nonlinearity of the bearing at close range as well as the impact of varying the modeled process noise intensity q.

The results of this simple experiment are in agreement with the findings of Haug and Williams [11]. In their study, the error performance for a variety of Cartesian and spherical tracking filters showed that, at close range, the tracks that relied on a Cartesian-to-spherical transformation tended to diverge, unlike the fully spherical filters. The results are also

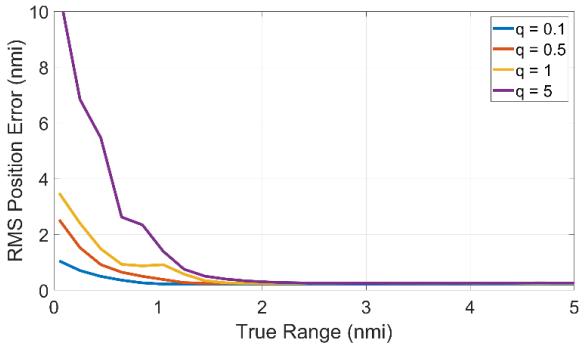

FIGURE 7. RMS position error plot for radially inbound target using various process noise intensity values (with units of nmi^2/sec^3), $\Delta t = 1$ second, $\sigma_R = 0.25$ nmi, and $\sigma_\theta = 1$ degree.

in agreement with the findings of Lerro and Bar-Shalom [16], who showed that a debiased converted measurement filter offers superior error and consistency performance compared to the Cartesian EKF.

V. SUMMARY

In this study, we derived and characterized the behavior of the PDF of a bearing random variable that is a function of two Gaussian distributed random variables (X and Y). The behavior of bearings at close range is often overlooked in other treatments of Kalman filters that use a Cartesian coordinate system to define the state vector and its dynamics. By using this PDF, filter designers can understand the range at which the Gaussian assumption for bearing may cause unwanted behavior in their target trackers. Alternatively, they may wish to use an different tracking method, such as an all-spherical EKF [11], a converted measurement filter [16], or an O2 algorithm [17] to reduce or eliminate the impact of these track divergence issues.

The PDF for the bearing was provided as well as its limiting behavior, which explains why the density appears Gaussian at long range. In this case, the approximate mean and variance were provided. At the near-range limit, the expected value of the bearing approaches zero. This property of density was then taken with knowledge of the Cartesian EKF to show that the position estimates behave poorly near the origin and can degrade the tracking performance, especially when coupled with poor selection of process noise.

REFERENCES

[1] V. J. Aidala and S. E. Hammel, "Utilization of modified polar coordinates for bearings-only tracking," *IEEE Trans. Autom. Control*, vol. AC-28, no. 3, pp. 283–294, Mar. 1983.
[2] Y. Bar-Shalom, X. R. Li, and T. Kirubarajan, *Estimation With Applications to Tracking and Navigation*. New York, NY, USA: Wiley, 2001.
[3] Y. Bar-Shalom, P. K. Willett, and X. Tian, *Tracking and Data Fusion: A Handbook of Algorithms*, Storrs, CT, USA: YBS, 2011.
[4] C. Caginalp and G. Caginalp, "The quotient of normal random variables and application to asset price fat tails," *Phys. A, Stat. Mech. Appl.*, vol. 499, pp. 457–471, Jun. 2018.
[5] G. Casella and R. L. Berger, *Statistical Inference*. Pacific Grove, CA, USA: Thomson Learning, 2002.
[6] I. S. Gradsheteyn and I. M. Ryzhik, *Table of Integrals, Series, and Products*. New York, NY, USA: Academic, 2007.
[7] P. D. Hanlon and P. S. Maybeck, "Characterization of Kalman filter residuals in the presence of mismodeling," *IEEE Trans. Aerosp. Electron. Syst.*, vol. 36, no. 1, pp. 114–131, Jan. 2000.
[8] A. J. Haug, "A yutorial on Bayesian estimation and tracking techniques applicable to nonlinear and non-Gaussian processes," MITRE, McLean, VA, USA, Tech. Rep. MTR 05W0000004, Jan. 2005.
[9] A. J. Haug, *Bayesian Estimation and Tracking: A Practical Guide*. Hoboken, NJ, USA: Wiley, 2012.
[10] A. J. Haug and K. R. Ford, "An end-point constrained extended Kalman filter for tracking maneuvering near-radially inbound targets," in *Proc. ISIF Conf. Inf. Fusion*, 2016, pp. 312–318.
[11] A. Haug and L. Williams, "A spherical constant velocity model for target tracking in three dimensions," in *Proc. IEEE Aerosp. Conf.*, Mar. 2012, pp. 1–15.
[12] D. V. Hinkley, "On the ratio of two correlated normal random variables," *Biometrika*, vol. 56, no. 3, pp. 635–639, Dec. 1969.
[13] R. E. Kalman, "A new approach to linear filtering and prediction problems," *Trans. ASME, D, J. Basic Eng.*, vol. 82, pp. 35–45, Oct. 1960.
[14] P. Kotaru and K. Sreenath, "Variation based extended Kalman filter on S_2," in *Proc. 18th Eur. Contr. Conf. (ECC)*, Naples, Italy, 2019, pp. 875–882.
[15] M. Krishnan, "The noncentral bivariate chi distribution," *SIAM Rev.*, vol. 9, pp. 708–714, Jun. 1967.
[16] D. Lerro and Y. Bar-Shalom, "Tracking with consistent converted measurements vs the EKF," *IFAC Proc.*, vol. 26, no. 2, pp. 365–368, 1993.
[17] T. Li, J. M. Corchado, J. Bajo, S. Sun, and J. F. De Paz, "Effectiveness of Bayesian filters: An information fusion perspective," *Inf. Sci.*, vol. 329, pp. 670–689, Feb. 2016.
[18] M. Mallick, *A Note on Bearing Measurement Model*. Berlin, Germany: Researchgate, 2018, doi: 10.13140/RG.2.2.13441.35681.
[19] K. V. Mardia and P. E. Jupp, *Directional Statistics*. Chichester NY, USA: Wiley, 2000.
[20] G. Marsaglia, "Ratios of normal variables and ratios of sums of uniform variables," *J. Amer. Statist. Assoc.*, vol. 60, no. 309, pp. 193–204, Mar. 1965.
[21] A. Papoulis, *Probability, Random Variables, and Stochastic Processes*, Boston, MA, USA: McGraw-Hill, 2002.
[22] A. Pollastri and F. Tornaghi, "Some properties of the arctangent distribution," *Stat. Appl.*, vol. 2, no. 1, pp. 3–18, 2004.
[23] S. O. Rice, "Mathematical analysis of random noise," *Bell Syst. Tech. J.*, vol. 24, no. 1, pp. 146–156, 1945.
[24] M. S. Schlosser and K. Kroschel, "Limits in tracking with extended Kalman filters," *IEEE Trans. Aerosp. Electron. Syst.*, vol. 40, no. 4, pp. 1351–1359, Oct. 2004.

KEVIN R. FORD (Member, IEEE) received the B.S. degree in mechanical engineering and the M.S. degree in electrical engineering from Lehigh University, Bethlehem, PA, USA, in 2010 and 2011, respectively. He is currently pursuing the Ph.D. degree in electrical engineering with a focus on nonlinear filtering and tracking with the Department of Electrical and Computer Engineering, University of Maryland, College Park, MD, USA.

Since 2011, he has been an Engineer with the Applied Physics Laboratory, Johns Hopkins University, Laurel, MD. His research interests include nonlinear filtering, complex system optimization, and radar modeling and simulation.

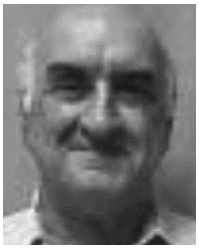

ANTON J. HAUG (Life Member, IEEE) was born in Sacramento, CA, in 1941. He received the B.S. degree in physics from the State University of New York, Stony Brook, in 1964, the M.A. degree in physics from the City University of New York, Queens College, Jamaica, NY, in 1968, and the Ph.D. degree in physics from the Catholic University of America, Washington, DC, in 1974.

He worked at the Applied Physics Laboratory, Johns Hopkins University, from 1968 to 1978, and again from 2009 until his retirement in 2018. He also worked at Planning Systems Incorporated, EG&G, Martin Marietta, Intermetrics, and MITRE. He also consulted for numerous companies from 1991 to 1997 and was an expert witness for the Howry & Simon law firm for four patent suites. At various times during his career he worked on acoustic and electromagnetic propagation modeling, acoustic scattering from submerged objects, active acoustic cancellation, conventional and adaptive signal processing, active and passive sonar design, and Bayesian estimation, tracking, and data fusion.